Physical Science International Journal

21(4): 1-20, 2019; Article no.PSIJ.19609
ISSN: 2348-0130

Nonlinear Finite Element Modelling for Reinforced Concrete Beams Retrofitted with FRP in Bending

Ihab Samir Abdou Ibrahim Mattar[1*]

[1]Arab Academy for Science, Technology and Maritime Transport, Department of Construction and Building, College of Engineering and Technology, Alexandria, Egypt.

Author's contribution

The sole author designed, analysed, interpreted and prepared the manuscript.

Article Information

DOI: 10.9734/PSIJ/2019/v21i430118
Editor(s):
(1) Dr. Xi Wu, Department of Mechanical Engineering, California Polytechnic State University, San Luis Obispo, USA.
(2) Dr. Christian Brosseau, Distinguished Professor, Department of Physics, Université de Bretagne Occidentale, France.
Reviewers:
(1) Jacob Nagler, Technion – Israel Institute of Technology, Israel.
(2) Dr. K. Nirmalkumar, Kongu Engineering College, India.
Complete Peer review History: http://www.sdiarticle3.com/review-history/19609

Original Research Article

Received 22 April 2015
Accepted 02 July 2015
Published 17 April 2019

ABSTRACT

For the purpose of simulating the behaviour of reinforced concrete (R.C)[1] beams retrofitted with fibre-reinforced polymers/plastics (FRP)[2] in bending, a finite element (FE)[3] modelling procedure has been developed throughout this paper. The FE software package ABAQUS CAE 6.11-3 was used. The data required for such modelling process are boundary conditions, geometric and material properties. Non-available material properties are obtained through experimentally verified numerical material models. FRP isotropic and orthotropic material models are compared; both models nearly yielded similar results. Also, perfect bond model and cohesive zone model for the interface between concrete and FRP have been compared. Unlike the perfect bond model, the cohesive zone model captured the debonding. The modelling procedure was validated through its application to R.C beams retrofitted with FRP in bending. The FE model results were compared to experimental results where both results were highly correlated. Such results include load-deflection curves and cracking pattern. The effect of sheet width and number of FRP layers is emphasized

[1] *R.C : Reinforced Concrete*
[2] *FRP : Fibre-reinforced polymers/plastics*
[3] *F.E : Finite element*

**Corresponding author: Email: dr_kremlin@hotmail.com;*

through performing a parametric study. Increasing sheet width is only effective at longer sheet lengths regarding increasing both; stiffness and load carrying capacity. Upon increasing the number of FRP layers, only shifting of the yielding point of reinforcement was noticed.

Keywords: ABAQUS; externally bonded; fiber reinforced polymer (FRP); finite element; reinforced concrete; retrofitting.

1. INTRODUCTION

For the purpose of enhancing the performance of concrete structures over prolonged periods of time, developing and studying various techniques required for strengthening such structures has become necessary. Such necessity has been induced in the field of Civil Engineering due to the fact that concrete structures are subjected to various factors such as creep, shrinkage, corrosion of reinforcement steel or even earthquakes which may cause the structure to fail in performing its function properly.

Various materials are used for the purpose of strengthening or reinforcing concrete structures where FRP (fibre reinforced polymers/plastics) has become one of those materials that is widely used in the recent years. The use of FRP for the purpose of strengthening or retrofitting reinforced concrete (R.C) structures can be achieved through its application as near surface mounted laminates, internally embedded reinforcement or as externally bonded sheets. The use of FRP in the form of externally bonded sheets for the purpose of retrofitting reinforced concrete structural elements such as beams, columns, slabs and girders has been discussed throughout various studies [8-11]. FRP, whose basic concepts regarding design and execution are discussed by Triantafillou [12]; has proven to be a reliable structural material in the field of reinforcing and strengthening concrete structures despite of its high initial cost and despite of being linear elastic in addition to the potentially damaging effects resulting from temperature, moisture, UV radiation, alkalinity and fire . Through its mechanical properties which include high strength, lightweight as well as being corrosion resistant and highly versatile, FRP has become an attractive material for the use in strengthening and reinforcing concrete structures.

Various research procedures have been carried out in order to investigate the effect of strengthening or retrofitting R.C beams with FRP where increased load carrying capacity and increased stiffness have been noticed in most cases. Various studies [13-17] emphasized the effect of using externally bonded carbon fibre reinforced polymers (CFRP) on enhancing the flexural and shear performance of R.C beams, in addition, various experimental procedures have proven that such method is more effective than using steel plates regarding cost and feasibility [18,19]. It should be noticed that despite of the debonding mode of failure discussed throughout various studies [20-24], using externally bonded CFRP or GFRP (glass fibre reinforced polymers) sheets enhanced the flexural capacity of R.C beams [25]. In addition, upon strengthening R.C beams with CFRP and GFRP laminates in flexure and shear respectively, an increase in the load carrying capacity of about 150% has been noticed [26]. Also, retrofitting R.C beams with CFRP laminates may increase its load carrying capacity by 170% [27]. Delayed tensile cracking in addition to increased stiffness has been noticed upon using CFRP sheets to strengthen R.C beams [28].

Regarding R.C beams retrofitted with FRP in bending, very few studies have been performed for the purpose of examining the behavior of such elements [29,30] compared to those performed on specimens externally strengthened with FRP [31-40]. It should be noticed that retrofitting R.C elements with FRP may induce certain types of failures which may cause shear failure, concrete debonding, CFRP delamination where such modes of failure are characterized by being brittle [41]. Also, shear stress concentration noticed at potential locations for development of shear cracking in concrete cause brittle debonding [42].

In order to achieve a wider field of applying FRP in strengthening and reinforcing existing concrete structures, applying various methods of investigation for the purpose of studying the composite action between FRP and concrete has become necessary. However, due to the fact that experimental procedures are expensive regarding both time and money, developing various modelling procedures regarding R.C

beams strengthened with FRP has become necessary. It should be noticed that the composite action that arise from the interaction between FRP and concrete caused the modelling procedure of elements strengthened or retrofitted with FRP to become a complex process due to the large number of variables included in the strengthening or retrofitting procedure. Various modelling procedures have been developed based upon the FEM (finite element method) [7,43,44] where such procedures considered FRP to be an isotropic material, thus neglecting the orthotropic material properties for FRP. It should also be noticed that the developed numerical procedures did not consider accurate modelling of the interface between concrete and FRP. Most numerical simulations neglected such interface, although various experimentally verified numerical material models for modelling the interface between concrete and FRP [45] were available. Most procedures considered either perfect bond between concrete and FRP or various estimations were used [2,46]. Accordingly, a need exists to apply the finite element method in order to develop a modelling procedure capable of simulating the behavior of reinforced concrete beams retrofitted with FRP in bending. Such modelling procedure aims towards predicting the future behavior of similar elements as well as studying the effect of retrofitting at low costs while considering orthotropic material properties of FRP in addition to capturing the debonding behavior based upon experimentally verified numerical material models.

This paper aims towards modelling the behavior of RC beams retrofitted with FRP in bending. A FE (finite element) model is prepared using the FE software package ABAQUS CAE 6.11-3 in conjunction with the available data which include loading conditions, material properties and boundary conditions. Model validation is carried out through applying the developed FE model to R.C beams retrofitted with FRP in bending and comparing the FE model results with experimental results. For the purpose of enhancing the retrofitting process, a parametric study is carried out.

2. THEORY/CALCULATION

In order to study the specified specimens a FE nonlinear analysis is carried out using the FE software package ABAQUS CAE 6.11-3.

2.1 Numerical Material Models

2.1.1 Concrete

Regarding the compressive stress-strain curve for concrete, the experimentally verified numerical method [5] is used as shown in Fig.1. As shown in Fig. 1, based upon maximum compression strength f_{cu}, this model obtains the stress-strain curve for concrete under uni-axial compression. The obtained stress-strain curve is up to 0.3 characteristic strength (f_{cu}) in the descending portion. It should also be noticed that this model follows a linear Stress-Strain relationship in accordance with HOOK's Law till 50 % $f_{cu.}$ Equations (1-4) emphasize the use of such model in order to obtain the compressive stress-strain curve for concrete.

$$\sigma_c = \left[\frac{(\eta*\beta)*(\varepsilon_c/\varepsilon_o)}{(\eta*\beta)-1+(\varepsilon_c/\varepsilon_o)^{(\eta*\beta)}}\right] * \sigma_{cu} \quad (1)$$

$$\beta = \frac{1}{1-[\sigma_{cu}/(\varepsilon_o * E_o)]} \quad (2)$$

$$\varepsilon_o = (8.9 * 10^{-5} * \sigma_{cu}) + 2.114 * 10^{-3} \quad (3)$$

$$E_o = (1.2431 * 10^2 * \sigma_{cu}) + (3.28312 * 10^3) \quad (4)$$

Where:

β: A material parameter which depends on shape of stress-strain diagram
ε_o: Strain at peak stress
ε_c: Strain at a given value for σ_c
E_o: Initial tangential modulus (Kip/in^2)
ε_d: Strain at 0.3 f_{cu} in the descending portion and is iteratively calculated using equation (1) at σ_c = 0.8 * σ_{cu}
σ_c: Compressive strength (Kip/in^2)
σ_{cu}: Ultimate compressive strength (Kip/in^2 → 1 MPa = 0.145037743 Kip/in^2)

Material parameter which depends on s_{cu} and is equal to one till a value of 62 MPa for f_{cu} [5].

The tensile behavior of concrete follows the model shown in Fig. 2 [4] where concrete follows a linear elastic behavior till maximum tensile strength (f_{ct}) after which the tensile softening behavior follows the relation shown in Fig. 2. Equations (5-7) [47] are used to obtain the values for f_{ct} (in MPa).

$$f_{ctk,min} = 0.95 * (0.1 * \sigma_{cu})^{2/3} \quad (5)$$

$$f_{ctk,m} = 1.4 * (0.1 * \sigma_{cu})^{2/3} \quad (6)$$

$$f_{ctk,max} = 1.85 * (0.1 * \sigma_{cu})^{2/3} \quad (7)$$

Where:

σ_{cu}: Ultimate compressive strength for concrete (MPa)

$f_{ctk,min}$: Minimum value for concrete tensile strength (MPa)

$f_{ctk,m}$: Mean value for concrete tensile strength (MPa)

$f_{ctk,max}$: Maximum value for concrete tensile strength (MPa)

δ_o: Crack opening displacement (mm)

G_f: Fracture energy (Nmm/mm^2)

In order to determine values for G_f (Nmm/mm^2) equation 8 [47] is used

$$G_f = G_{fo} * (0.1 * \sigma_{cu})^{0.7} \quad (8)$$

Where:

σ_{cu}: Ultimate compressive strength for concrete (MPa)

G_{fo}: Base value for fracture energy (Nmm/mm^2) and depends on maximum aggregate size as shown in table 1.

2.1.2 Reinforcement

Reinforcement is modelled as an elastic perfectly plastic material with identical behavior in tension and compression as shown in Fig. 3.

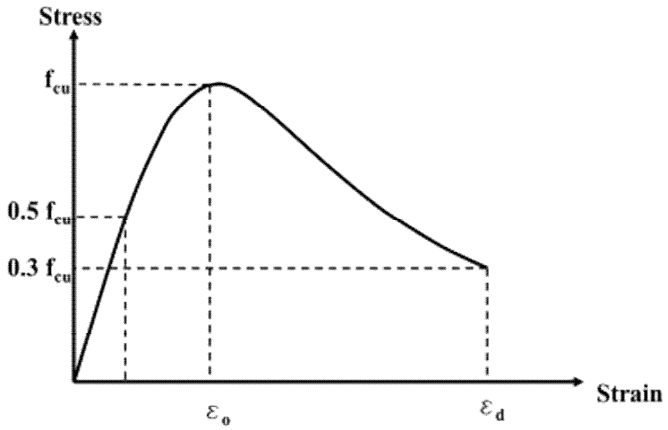

Fig. 1. Compressive Stress-Strain relationship for concrete [5]

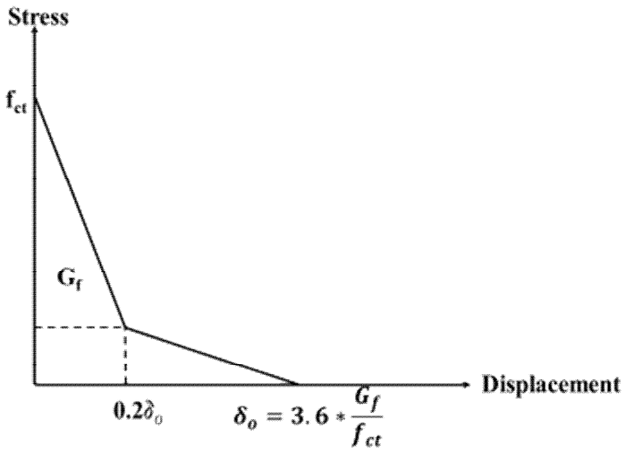

Fig. 2. Softening curve for concrete under uni-axial tension [4]

2.1.3 FRP

Two material models are available for FRP. Although FRP is an orthotropic material, thus it is more convenient to use the orthotropic material model. However, it must be noticed that since the composite is mainly stressed in the fiber direction, therefore, the modulus in the fiber direction is more important and accordingly using the isotropic material model is acceptable. In order to model FRP using the orthotropic material model, rule of mixtures and inverse rule of mixture [48] are used as shown in equations (9-10)

$$E_1 = (V_f * E_f) + (V_m * E_m) \quad (9)$$

$$\frac{1}{E_2} = \frac{1}{E_3} = \frac{V_f}{E_f} + \frac{V_m}{E_m} \quad (10)$$

Where:

E_1: Modulus of elasticity in fibre direction (MPa)
E_2: Modulus of elasticity normal to fibre direction (MPa)
E_3: Modulus of elasticity normal to fibre direction (MPa)
V_f: Fibre volume fraction
V_m: Matrix volume fraction
E_f: Modulus of elasticity for fibre (MPa)
E_m: Modulus of elasticity for matrix (MPa)
Regarding Poisson ratio (ν_{12} and ν_{13}) and shear modulus (G_{12} and G_{13}), their values can be obtained using equations (11-12) [48].

$$\nu_{12} = \nu_{13} = (V_f * \nu_f) + (V_m * \nu_m) \quad (11)$$

$$\frac{1}{G_{12}} = \frac{1}{G_{13}} = \frac{V_f}{G_f} + \frac{V_m}{G_m} \quad (12)$$

Where

ν_m: Poisson ratio for matrix
ν_f: Poisson ratio for fibre
V_f: Fibre volume fraction
V_m: Matrix volume fraction
G_f: Shear modulus for fibre (MPa)
G_m: Shear modulus for matrix (MPa)
ν_{12}, ν_{13} and ν_{23} are set to 0.3, 0.3 and 0.45 respectively, while G_{12}, G_{13} and G_{23} are set to 5.2 GPa, 5.2 GPa and 3.4 GPa respectively.

2.1.4 Adhesive

Fig. 4 shows the cohesive zone model [3] used to model the adhesive

Where:

τ: Effective traction (traction stress) (MPa)
δ: Effective displacement/Separation (mm)
δ_o: Slip corresponding to ultimate bond stress (mm)
G_{cr}: Fracture energy and is resembled by the area under the curve. Where its value ranges from 300J/m^2 up to 1500J/m^2, an average value of 900J/m^2 is used
K_o: Initial Stiffness for adhesive (N/mm^3) and is obtained using equation 13.

$$k_o = \frac{1}{(t_i/G_i)+(t_c/G_c)} \quad (13)$$

t_i: resin thickness : 1 mm
t_c: effective thickness of concrete whose deformation takes part in the interfacial slip : 25 mm (usually taken as value of concrete cover)
G_i: shear modulus for resin: 665 MPa
G_c: shear modulus for concrete: 10800 MPa
τ_{max}: Maximum shear stress (local strength of the material) (MPa) and is obtained using equation 14.

$$\tau_{max} = 1.5 * \beta_w * f_{ct} \quad (14)$$

f_{ct}: Concrete tensile strength (MPa)

$$\beta_w = \sqrt{(2.25 - \frac{w_{frp}}{w_b})/(1.25 + \frac{w_{frp}}{w_b})} \quad (15)$$

w_{frp}: FRP plate width (mm)
w_b: Concrete width (mm)
In cases where FRP sheets are used for strengthening/retrofitting in shear, wb is replaced with spacing of FRP strips (s_{frp}) (mm)

The quadratic traction function [49] is used to model damage initiation, according to equation 16 damage initiation occurs when nominal stress ratios equals one.

$$\left\{\frac{\sigma_n}{\sigma_n^o}\right\}^2 + \left\{\frac{\tau_s}{\tau_s^o}\right\}^2 + \left\{\frac{\tau_t}{\tau_t^o}\right\}^2 = 1 \quad (16)$$

σ_n:: adhesive tensile stress in pure normal mode (MPa)
σ_n^o: Peak value for adhesive tensile stress in pure normal mode its value is taken as f_{ct} (MPa)
τ_s: adhesive shear Stress in first shear direction (MPa)
τ_s^o : Peak value for adhesive shear Stress in first shear direction its value is taken as τ_{max} (MPa)
τ_t: adhesive shear Stress in second shear direction (MPa)
τ_t^o : Peak value for adhesive shear Stress in second shear direction its value is taken as τ_{max} (MPa)

Table 1. Base Values for fracture energy [44,47]

d_{max} (mm)	G_{fo} (Nmm/mm^2)
8	0.025
16	0.03
32	0.058

Equations (17-20) emphasize the modelling of the damage evolution in terms of energy release. Benzaggah–Kenane fracture criterion [49,50] is used to express the relation between fracture energy and mode mix, such criterion is useful in case critical fracture energy in first and second shear directions are equal ($G_s^c = G_t^c$) . The relative proportions of normal and shear deformation are quantified by the mode mix of the deformation fields in the cohesive zone [49,50]

$$G_n^c + (G_s^c - G_n^c)\left\{\frac{G_{Ss}}{G_T}\right\}^{h} = G^c \quad (17)$$

Where:

G_n^c: Critical fracture energy in normal direction taken as G_f (Nmm/mm^2)
G_s^c: Critical fracture energy in first shear direction taken as G_{cr} (Nmm/mm^2)
G_t^c: Critical fracture energy in second shear direction taken as G_{cr} (Nmm/mm^2)
G^c: Energy dissipated due to failure (Nmm/mm^2) (18)

(19)

(20)

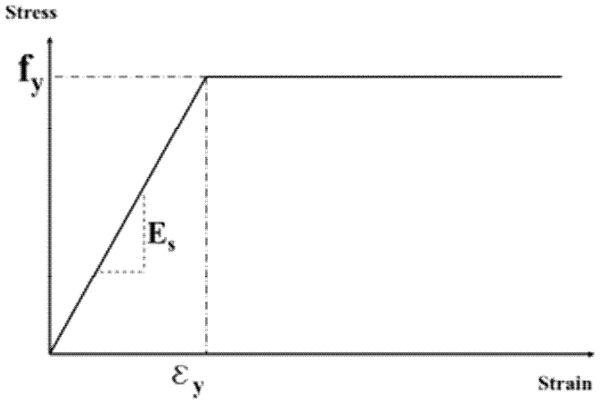

Fig. 3. Stress – Strain behavior for reinforcement [6]

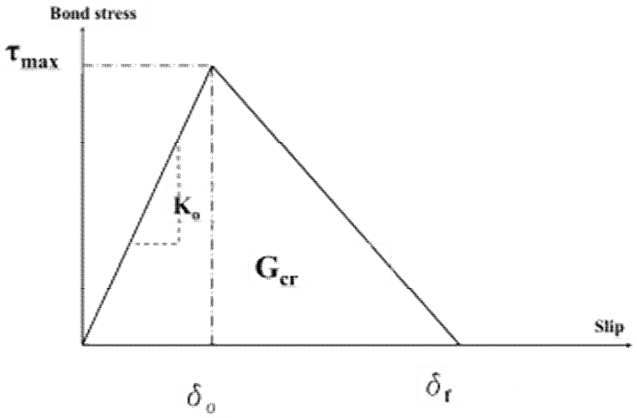

Fig. 4. Billinear model for bond slip curve [3]

$$G_s^c = G_t^c \quad (18)$$

$$G_{Ss} = G_s + G_t \quad (19)$$

$$G_T = G_n + G_s \quad (20)$$

η: A material parameter taken as 1.45
G_n: refer to the work done by the traction and its conjugate separation in the normal direction (Nmm)
G_s: refer to the work done by the traction and its conjugate separation in the first shear direction (Nmm)
G_t: refer to the work done by the traction and its conjugate separation in the second shear direction (Nmm)

2.2 Numerical Simulation

Abaqus provides three material models that allow the user to model reinforced concrete, these models are concrete smeared cracking model, brittle cracking model and concrete damaged plasticity model. The smeared cracking model was avoided in order to avoid convergence issues; also, the brittle cracking model is avoided, since it is only available for use in abaqus explicit that is mainly for dynamic analysis. Accordingly, using the concrete damaged plasticity model has proven to be the most appropriate not only for the reasons stated above, but also because it can be used in both abaqus/standard and abaqus/explicit, thus allowing the transfer of results between both [49]. Regarding the concrete damaged plasticity model, the direction of the vector normal to the crack plane is assumed to be parallel to the direction of the maximum principal plastic strain [49]. In addition, the concrete damaged plasticity model does not have a cracking notation, however, cracking is considered to initiate at points where the maximum principal plastic strain is positive [51].Also such model assumes that the two main concrete failure mechanisms are tensile cracking and compressive crushing [52,53].

C3D4 mesh elements are used for concrete. In addition, the same element type is used for FRP in case perfect bond model is used. However, in case the cohesive zone model interaction property is used to model interaction between concrete and FRP, C3D8R mesh elements are used to model FRP. Cohesive zone model is used only for externally bonded sheets; otherwise, separation of concrete cover is the main mode of failure [54]. Therefore, perfect bond model is used to model the interaction between concrete and FRP for cases other than externally bonded sheets. T3D2 mesh elements are used for reinforcement steel where it should be noticed that interaction between concrete and reinforcement is obtained through the embedded element constraint. Nonlinear equilibrium equations are solved using Newton's method. Two gaps each is 0.1mm width and 10 mm depth were used to model the pre-crack where such gaps are distanced 40mm from each other; each is located at 20 mm from beam center at either side.

3. MODEL VALIDATION

In order to validate the FE model it was necessary to apply such modelling process on specimens previously studied through experimental procedures. Specimens studied by Obaidat.Y [1] were modelled using the above procedure. The experimental procedure performed by Obaidat Y. [1] is shown in Fig. (5-6), where insufficient flexural reinforcement induces flexural failure. Specimens included in this experimental procedure consist of a control beam (RF) and three retrofitted beams (RF1, RF2 and RF3) with sheet width 50mm. Material properties are given in table 2. According to the experimental procedure performed by Obaidat.Y [1], the mode of failure noticed is FRP debonding. Therefore, values for (τ_s and τ_t) are reduced from 4.1 MPa to 1.5 MPa since a value of 4.1 MPa induced a different mode of failure that is either FRP rupture or concrete crushing.

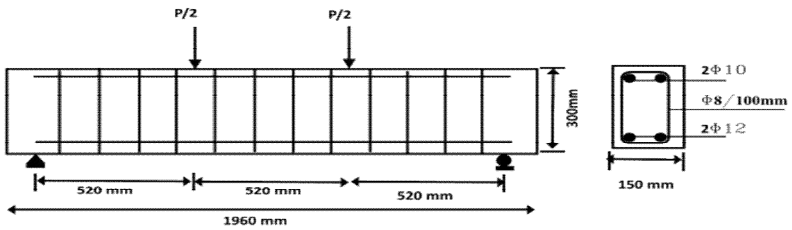

Fig. 5. Test setup and specimen details for control specimen RF [1]

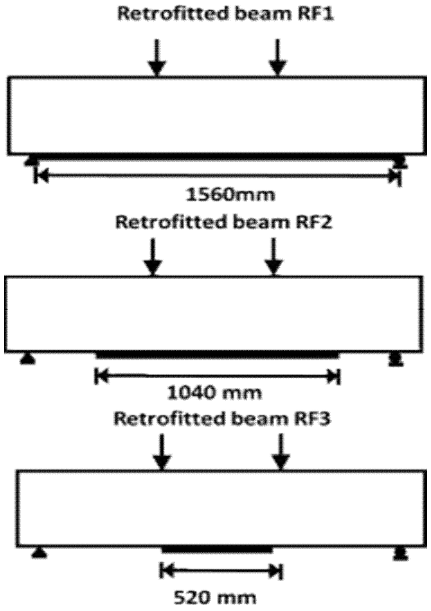

Fig. 6. Retrofitted beams RF1,RF2 and RF3 [1]

In addition, the specimens examined by Kang et al. [7] have been used in order to validate the proposed modelling procedure. Where a number of reinforced concrete beams designed to fail in bending were strengthened with FRP using near surface mounted laminates. The experimental program was performed on a control specimen (Control) in addition to four specimens (Type 1-1, Type 1-2, Type 2-1 and Type 2-2) as shown in Fig. 7. Material are given in Table 3.

4. RESULTS

4.1 Load-displacement Curves

Regarding the experimental program performed by Obaidat Y [1], load displacement curve for specimen RF is shown in Fig.7, where FE model result is in agreement with experimental results. Simulations performed on specimen RF1 are for the purpose of examining various modelling criteria available. Accordingly, four simulations were performed on specimen RF1 where the cohesive zone model (CZM)[4] is used once in conjunction with the isotropic (Iso) [5] material model for FRP and once with the orthotropic (Ortho)[6] material model for FRP. While the other two simulations used the perfect bond model (PBM)[7] once in conjunction with FRP isotropic material model and once in conjunction with FRP orthotropic material model. Results for specimen RF1 are shown in Fig. 8. The obtained results from the FE model indicated that the orthotropic model and isotropic model for FRP both yielded similar results. However, the perfect bond model overestimates the load carrying capacity of the beam after appearance of cracks which is due to the fact that the perfect bond model does not consider the shear strain between concrete and FRP where such shear strain increases upon appearance of cracks and therefore increasing the load carrying capacity of the beam. Since debonding failure cannot be captured through the perfect bond model; perfect bond model cannot capture softening behavior of the beam, therefore analysis continues till another mode of failure occurs which in this case may be shear flexural crack failure or FRP rupture. Based upon simulations performed on specimen RF1, specimens RF2 and RF3 were modelled using cohesive zone model in conjunction with the isotropic material model for FRP where load displacement curves for both pecimens are in agreement with experimental procedures as indicated in Figs. 9-10.

[4] *CZM : Cohesive zone model*
[5] *Iso : Isotropic*
[6] *Ortho : Orthotropic*
[7] *PBM : Perfect bond model*

Table 2. Material properties for specimens examined by Obaidat Y. [1]

Material	Property	Value
Steel	Yeild Stress	507 MPa
	Modulus of elasticity	210000 MPa
	Poisson ratio [a]	0.3
	Density [a]	7.85 e-9 t/mm^3
Concrete	Characteristic Strength	30 MPa
	Density [a]	2.5 e-9 t/mm^3
	Poisson ratio [a]	0.2
	Fracture Energy (G_f) [b]	0.122 Nmm/mm^2
	Modulus of elasticity (E_c)[b]	26365 MPa
	Tensile Strength (f_{ct})[b]	2.445 MPa
FRP	Modulus of Elasticity (E_1)	165000 MPa
	Modulus of Elasticity (E_2)[b]	9669 MPa
	Modulus of Elasticity (E_3)[b]	9669 MPa
	Em[b]	2500 MPa
	Ef[b]	219167 MPa
	Vm	25%
	Vf	75%
	v_{12}	0.3
	v_{13}	0.3
	v_{23}	0.45
	G_{12}	5200 MPa
	G_{13}	5200 MPa
	G_{23}	3400 MPa
	Density, t/mm^3	1.55 e-9 t/mm^3
	Poisson ratio	0.3
Adhesive	K_o [b]	508 N/mm^3
	σ_n [b]	2.445 MPa
	τ_s [b]	4.1 MPa
	τ_t [b]	4.1 MPa
	G_n [b]	0.12 Nmm/mm^2
	G_s [b]	0.9 Nmm/mm^2
	G_t [b]	0.9 Nmm/mm^2

[a] *Assumed values as the values for density and Poisson ratio were not specified in the original procedure.*
[b] *Material Properties obtained from material models discussed throughout the analytical procedure*

Load displacement curves for the experimental program performed by Kang et al. [7] are shown in Fig. 12-16. The FE model results are in agreement with the experimental results. The FE model predicts excessive ductile behavior among all specimens in addition to a slightly stiffer behavior, where excessive stiffness is indicated by the slight shift in the yielding point of reinforcement. Variation on load carrying capacity between FE model and experimental program has an average variation of 14%. The huge increase in load carrying capacity and ductility for specimens “Type 2-1” and “Type 2-2” may be due to assuming a perfect bond between concrete and FRP which indicates that failure for such specimens did not occur due to concrete cover seperation but is due to debonding. FE model results and experimental results are in agreement for the first part of the curve. However, upon appearance of cracks, the perfect bond model fails to capture the softening behavior of the beam and also cannot capture debonding resulting in overstimating ductility and load carrying capacity. This is due to the fact that the perfect bond model fails to consider the shear strain between concrete and FRP, where such shear strain increases upon appearance of cracks, thus decreasing beam stiffness.

4.2 Cracking Pattern

The cracking pattern for the control specimen RF according to experiments and FE model is shown in Fig.17.Regarding specimen RF1, as shown in Fig.18, the debonding mechanism is captured and is in agreement with debonding noticed in the experimental procedure shown in Fig.12. Cracking patterns for all specimens are in agreement with experimental results indicating that the FE model can properly capture the fracture mechanism.

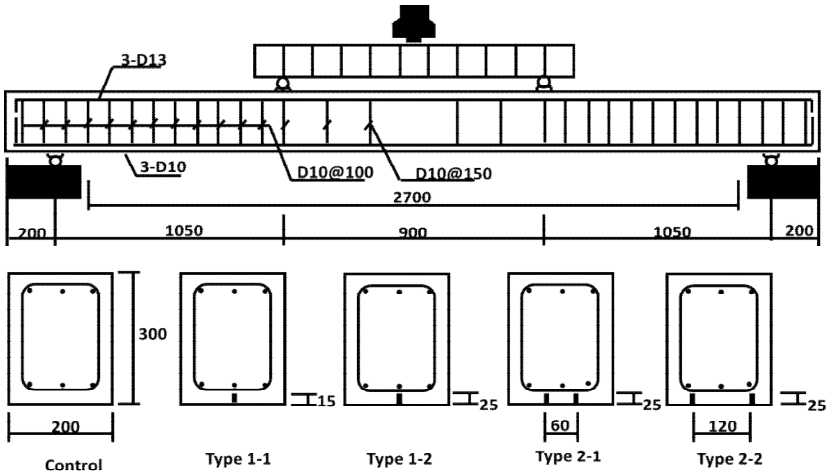

Fig. 7. Experimental program performed by Kang et al. [7]

Table 3. Material properties for specimens examined by Kang et al. [7]

Material		Property	Value
Reinforcement	**General Reinforcement Properties**	**Poisson ratio (n)***	0.3
		Density*	7.85 t/m^3
	D 10	Yeild Stress (f_y)	425 MPa
		Modulus of Elasticity (E_s)	200 GPa
	D 13	Yeild Stress (f_y)	480 MPa
		Modulus of Elasticity (E_s)	200 GPa
Concrete		Characteristic Strength (f_c')	32 MPa
		Modulus of Elasticity (E_c)**	26.6 GPa
		Tensile Strength (f_{ct})	2.95 MPa
		**Fracture Energy (G_f) ** **	0.12 Nmm/mm^2
		Density*	2.5 t/m^3
		Poisson ratio (n)*	0.2
FRP		Density, t/mm^3*	1.55 e-9 t/mm^3
		Poisson ratio	0.3
		Modulus of Elasticity *	165GPa

** Assumed values as the values for Poisson ratio and density were not specified in the original procedure*
*** Material Properties obtained from numerical material models discussed throughout the analytical procedure*

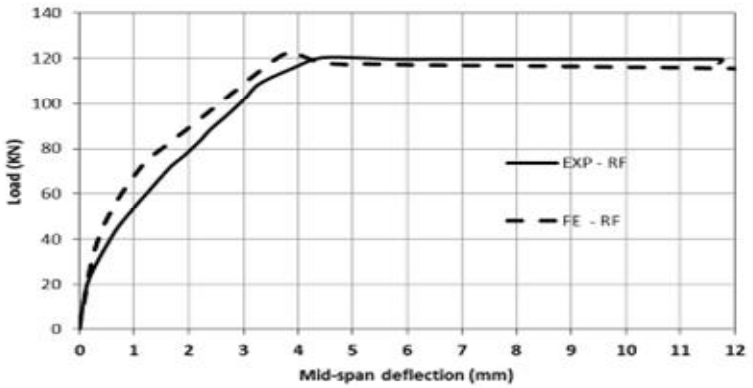

Fig. 8. Load displacement curve for specimen RF obtained from experiments [1] and FE model

Cracking patterns for the specimens by Kang et al. [7] are shown in Fig. 19. Experimental results regarding the cracking pattern are not available in the performed experimental procedure, yet the obtained cracking patterns are in agreement with the typical cracking pattern of flexure failure specimens which indicate that the FE model can capture the fracture mechanism. Debonding could not be captured due to the fact that the perfect bond model cannot capture debonding fracture mode of failure. The proposed modelling process is further validated through cracking confinement which is due to the strengthening procedure as shown in Fig. 19. Compared to the cracking pattern of the control specimen, upon enhancing the strengthening procedure more cracks develop with decreased width.

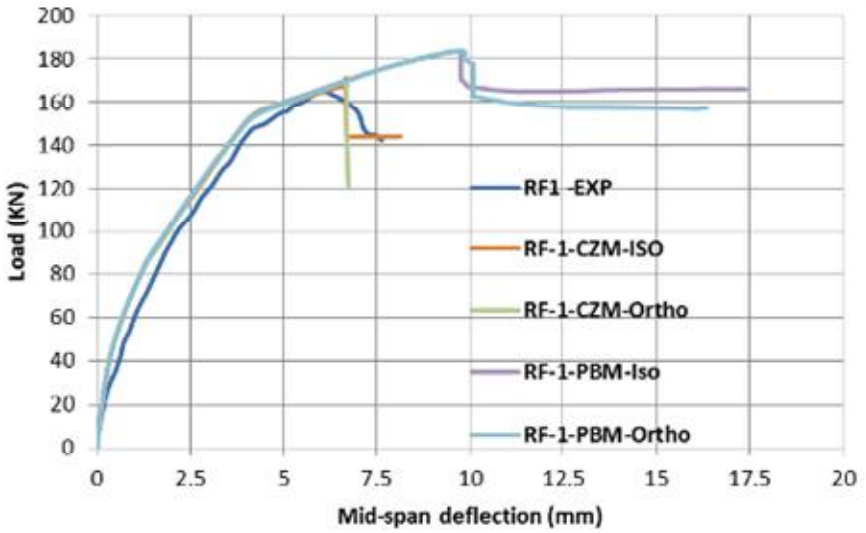

Fig. 9. Load displacement curve for specimen RF1 obtained from experiments [53] and FE model

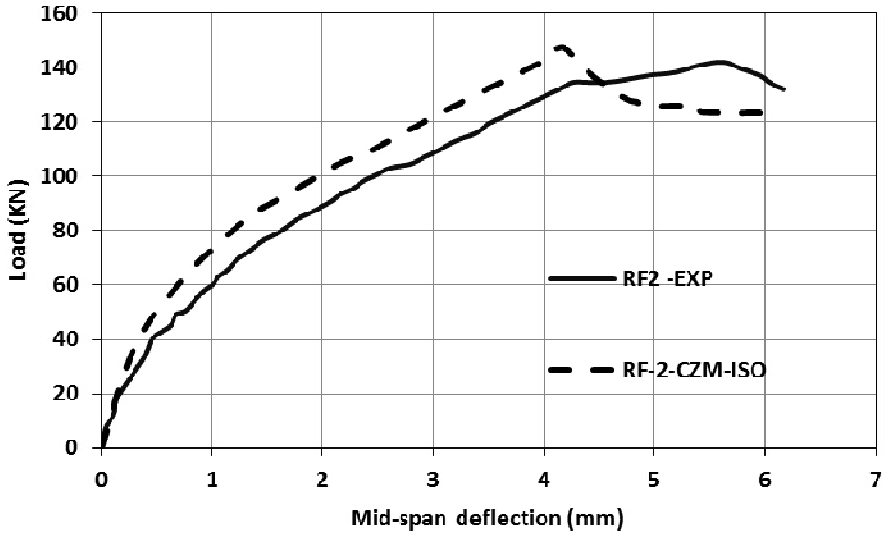

Fig. 10. Load displacement curve for specimen RF2 obtained from experiments [1] and FE model

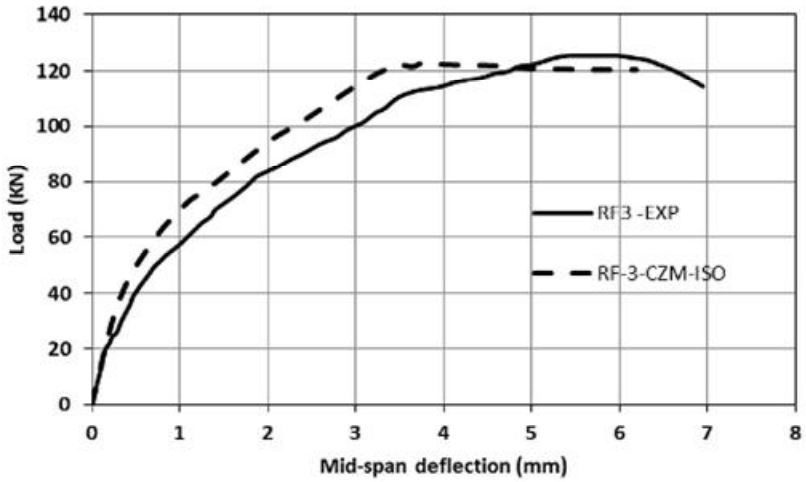

Fig. 11. Load displacement curve for specimen RF3 obtained from experiments [1] and FE model

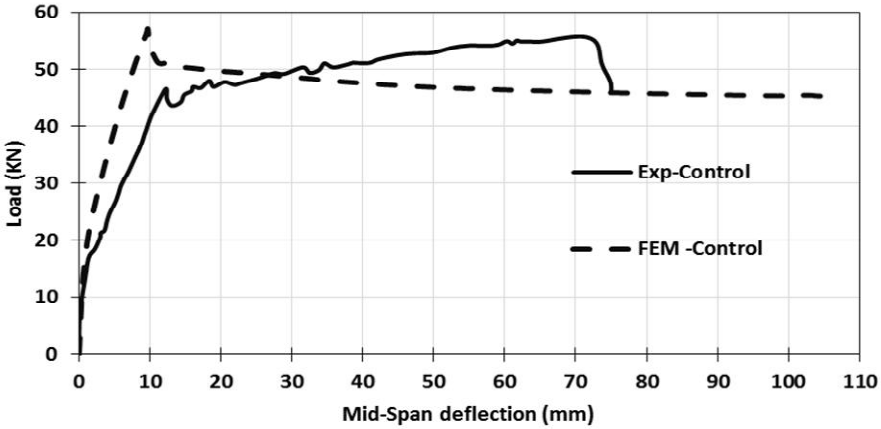

Fig. 12. Laod displacement curves for specimen "Control" obtained from experiments [7] and FE model

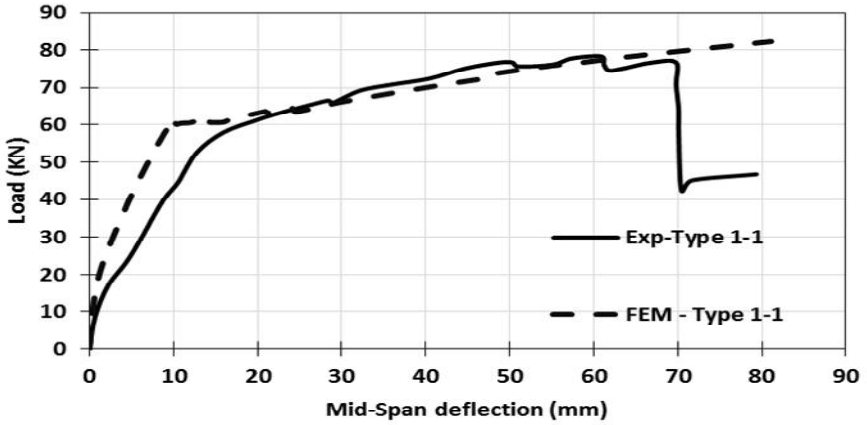

Fig. 13. Laod displacement curves for specimen "Type 1-1l" obtained from experiments

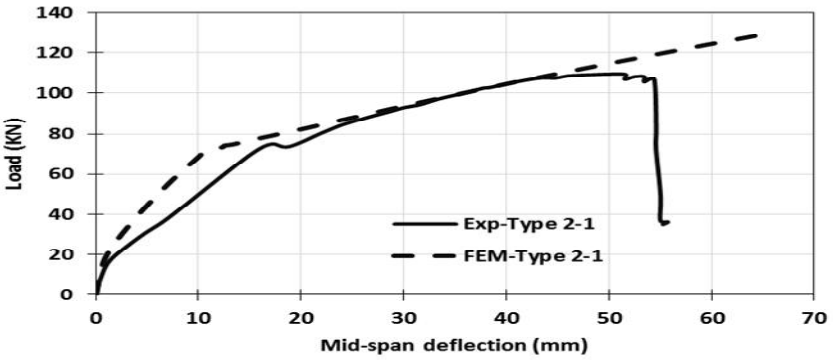

Fig. 14. Laod displacement curves for specimen "Type 2-1" obtained from experiments [7] and FE model

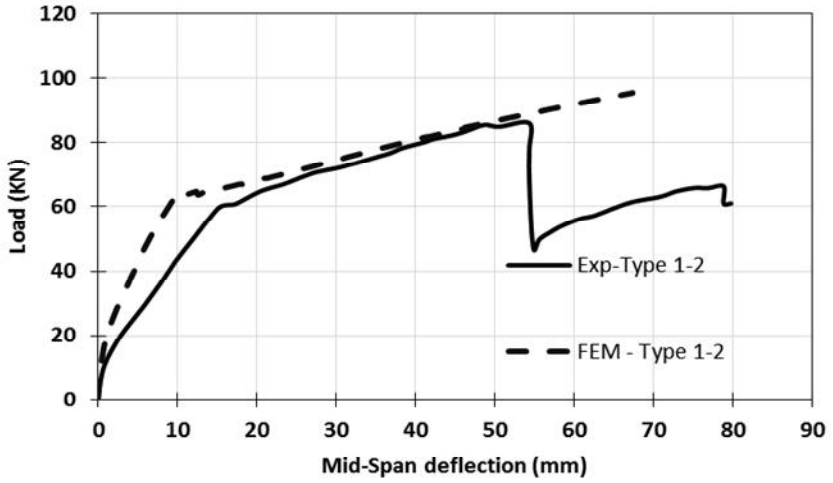

Fig. 15. Laod displacement curves for specimen "Type 1-2" obtained from experiments [7] and FE model

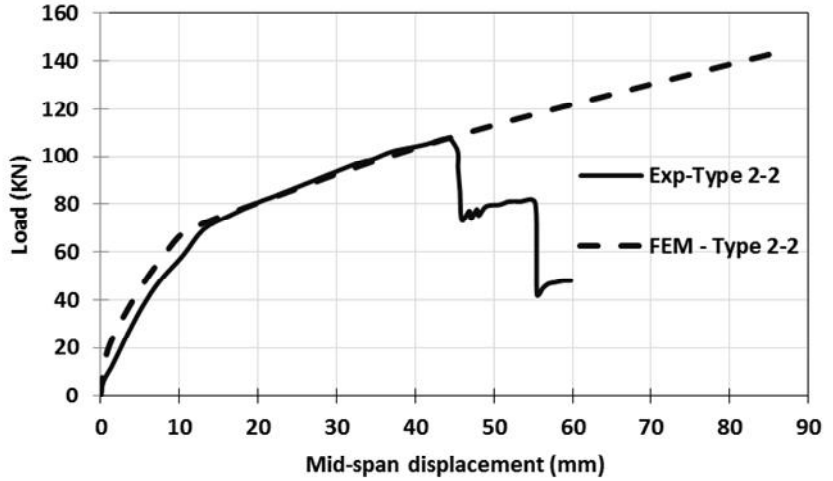

Fig. 16. Laod displacement curves for specimen "Type 2-2" obtained from experiments [7] and FE model

5. PARAMETRIC STUDY

5.1 Sheet Width

For the purpose of studying the effect of sheet width regarding specimens retrofitted with externally bonded sheets, a number of simulations were performed on specimens RF1,RF2 and RF3 [1] where each specimen is modelled with sheet width 100 mm and 150 mm. Table 3 shows the arrangement of the parametric study where results are shown in Figs. 20-22.

Where:
P_{ucb}: Ultimate load for control specimen (KN)
P_{urs}: Ultimate load for retrofitted specimen (KN)
W_{frp}: FRP sheet width (mm)
W_b: Beam width (150mm)

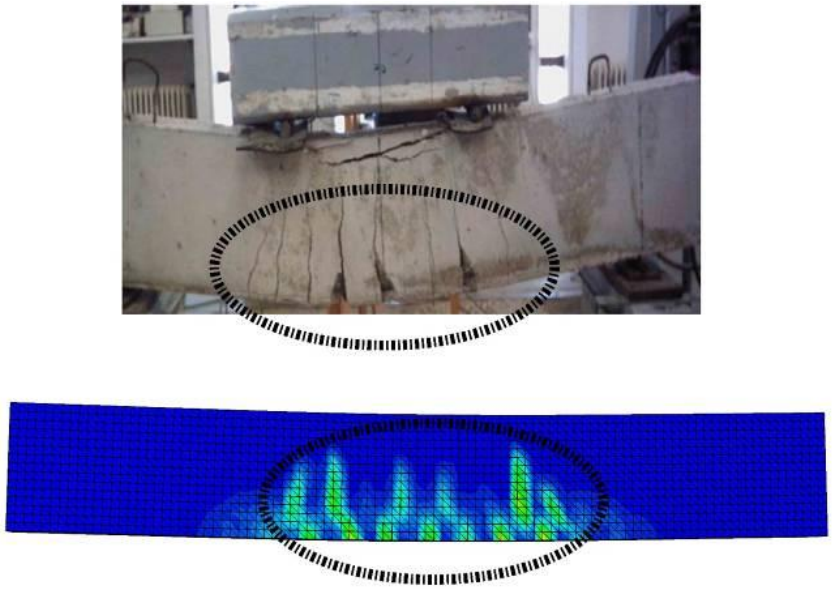

Fig. 17. Cracking pattern for specimen RF obtained from experiments [1] and FE model

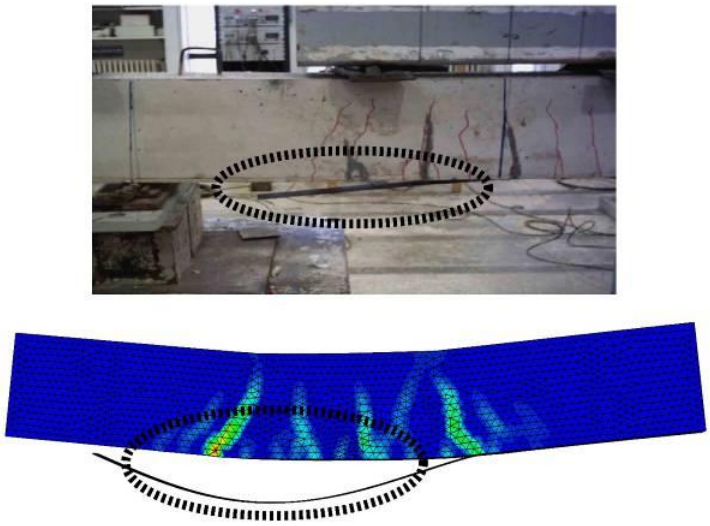

Fig. 18. Cracking pattern-debonding for retrofitted specimens in group RF according to experiments [1, 2] and FE model

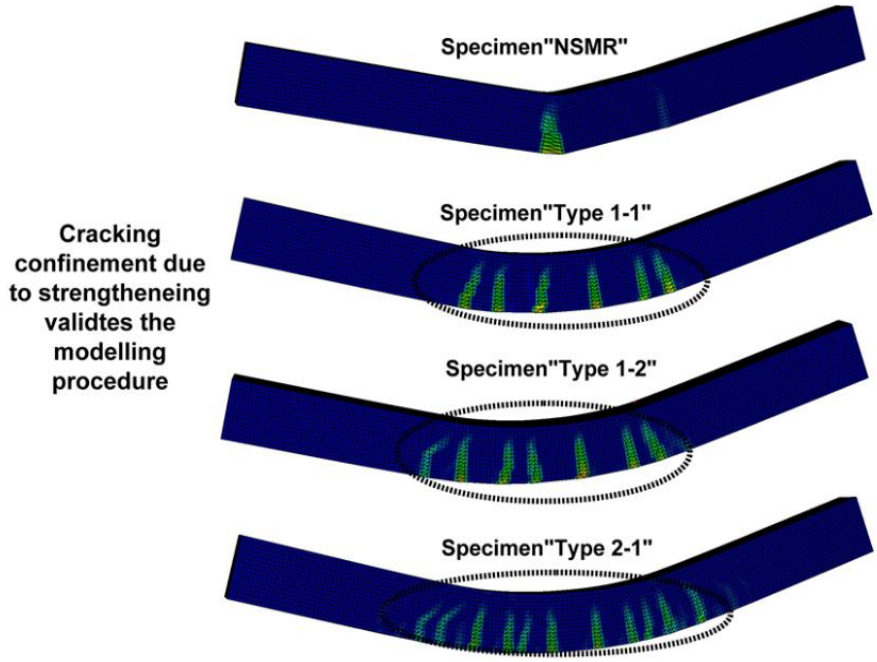

Fig. 19. Cracking pattern for specimens examined by Kang et al. [7]

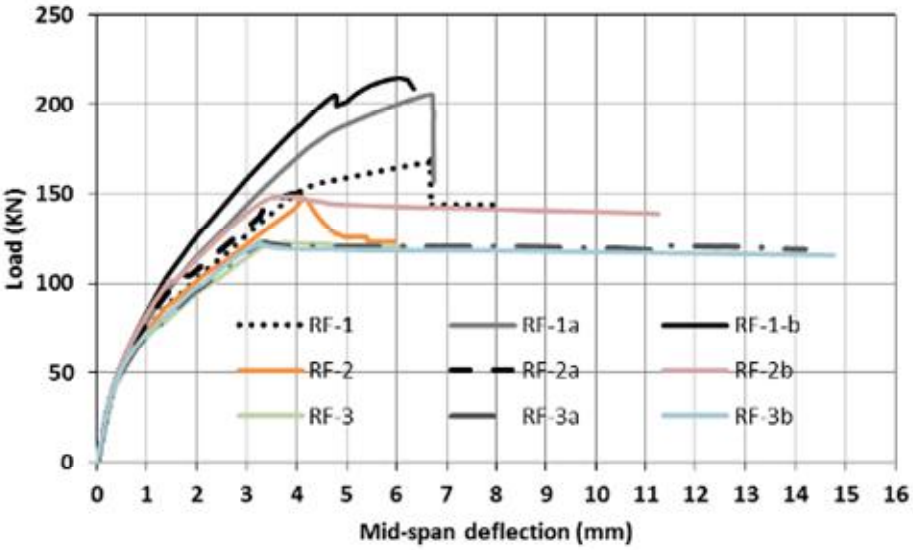

Fig. 20. Load displacement curves for various simulations performed on specimens RF1, RF2 and RF3

The obtained results indicate that increasing sheet width had the most effect at longer sheet lengths which is due to the fact that longer sheets had more anchorage length outside the maximum moment region leading to lower stress concentration and therefore debonding occurred at later stages during the loading process. Also the effect of increasing sheet width at lower sheet lengths is barely noticed. Increasing sheet width increased the effect of retrofitting procedure through delaying the FRP separation.

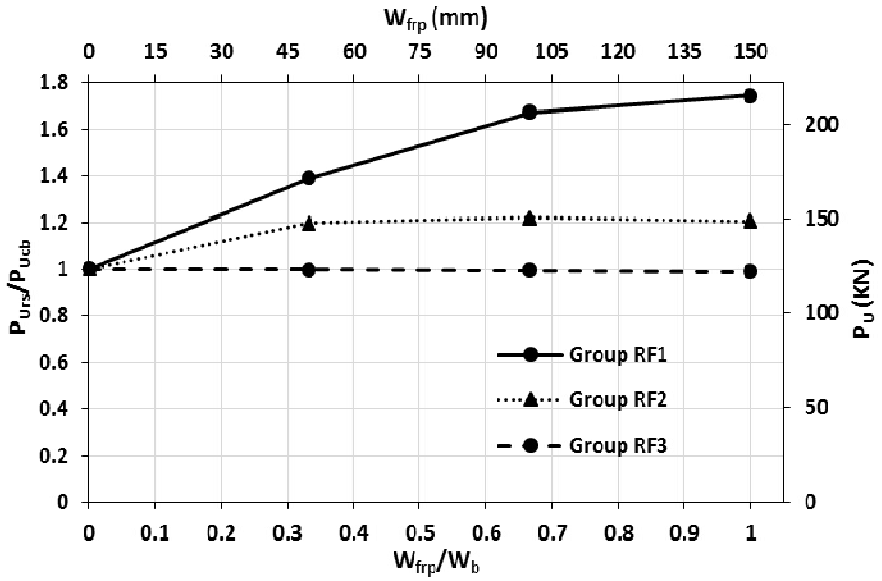

Fig. 21. Increase rate of ultimate load vs. sheet width for retrofitted specimens

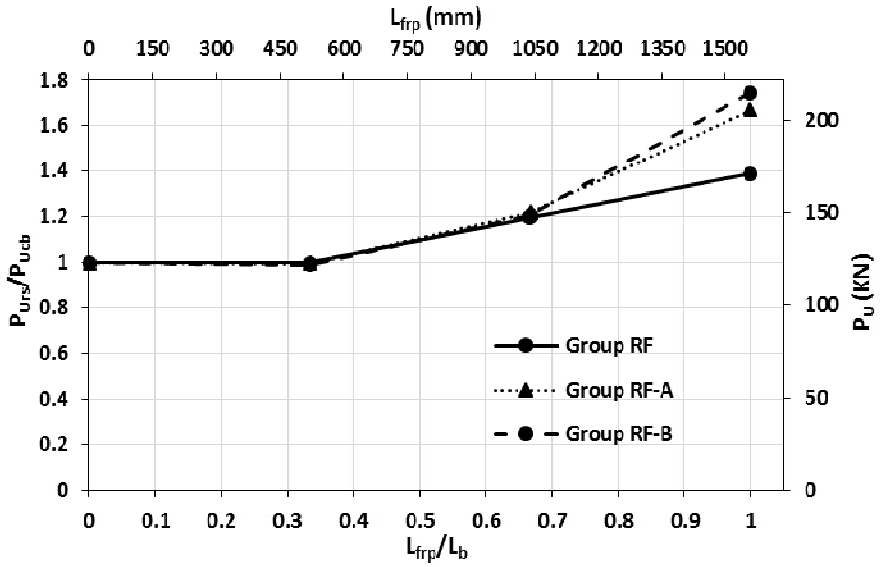

Fig. 22. Increase rate of ultimate load vs. sheet length for retrofitted specimens

5.2 Number of FRP Layers

In order to study the effect of the number of FRP layers on the beam behavior, a number of simulations were performed on the retrofitted specimen RF1b whose arrangement is emphasized in Table 4. Specimens RF1b-t2 and RF1b-t3 were modelled with two and three FRP layers respectively. The results shown in Fig. 23 indicate that increasing the number of layers resulted in increased stiffness and decreased ductility where such results are in accordance with the results achieved by Hashemi et al. [55] and Emadi et al. [56]. Changing the number of FRP layers shifted the yielding point yet the load carrying capacity remained unchanged.

Table 4. Arrangement for parametric study performed on specimens RF1, RF2 and RF3 regarding sheet width

Specimen		Sheet width (mm)	Sheet length (mm)
RF 1	*RF 1a*	100	1560
	RF 1b	150	1560
RF 2	*RF 2a*	100	1040
	RF 2b	150	1040
RF 3	*RF 3a*	100	520
	RF 3b	150	520

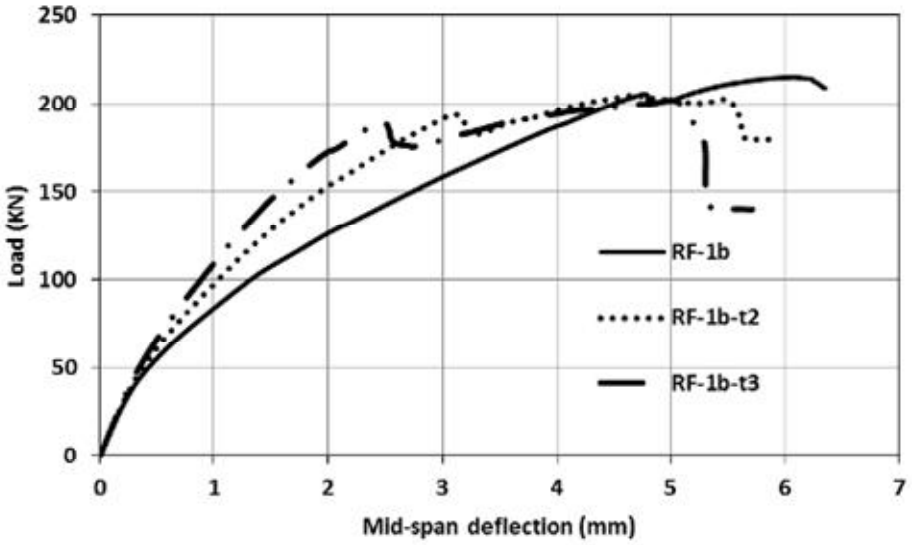

Fig. 23. Load displacement curves for various simulations performed on specimen RF-1b emphasizing the effect of number of FRP layers

6. CONCLUSION

For the purpose of simulating the behavior of R.C beams retrofitted with FRP in bending, a non-linear finite element modelling procedure has been developed. Such modelling procedure has been applicatied to R.C beams retrofitted with FRP in bending where validation has been achieved through comparing the results obtained from the FE model with those available from the experimental procedure. Finally, a parametric study has been carried out in order to study the effect of sheet width and number of layers for specimens retrofitted with externally bonded sheets. The following is to be noticed:

1- Agreement between load displacement curves obtained from FE model and experimental procedure indicate that the FE model can properly simulate the behavior of the specimens under study.

2- Cracking pattern obtained from FE model indicate that the proposed FE model can properly capture the fracture mechanism, such conclusion is verified through comparing cracking pattern obtained from FE model with that available from the experimental procedure.

3- Slight differences were noticed between isotropic material model and orthotropic model for FRP, which indicates that the use of isotropic material model is accepted.

4- Perfect bond model cannot capture the debonding failure and therefore overestimating the behavior of the examined specimen. Accordingly, the cohesive zone model is recommended for modelling specimens with externally

bonded sheets in case debonding failure is the dominant mode of failure.

5- Regarding the parametric study:

- Increasing the sheet width increased the effect of the retrofitting procedure through delaying the FRP separation; however, such effect is only noticed at longer sheet lengths with more anchorage lengths outside the maximum moment region.

- Increased stiffness and decreased ductility are noticed upon increasing the number of FRP layers, where the load carrying capacity remained unchanged yet shifting of the yielding point has been noticed.

COMPETING INTERESTS

Author has declared that no competing interests exist.

REFERENCES

1. Obaidat YT, Heyden S, Dahlblom O, Abu-Farsakh G, Abdel-Jawad Y. Retrofitting of reinforced concrete beams using composite laminates. Construction and Building Materials. 2011;25:591-597.
2. Hu HT, Lin FM, Jan YY. Nonlinear finite element analysis of reinforced concrete beams strengthened by fiber-reinforced plastics. Composite Structures. 2004;63: 271-281.
3. Lu X, Teng J, Ye L, Jiang J. Bond–slip models for FRP sheets/plates bonded to concrete. Engineering Structures. 2005;27: 920-937.
4. Hillerborg A. The theoretical basis of a method to determine the fracture energy G F of concrete. Materials and Structures. 1985;18:291-296.
5. Hsu L, Hsu CT. Complete stress—strain behaviour of high-strength concrete under compression. Magazine of Concrete Research. 1994;46:301-312.
6. Ibrahim AM, Mahmood MS. Finite element modeling of reinforced concrete beamsstrengthened with FRP laminates. European Journal of Scientific Research. 2009;30:526-541.
7. Kang JY, Park YH, Park JS, You YJ, Jung WT. Analytical evaluation of RC beams strengthened with near surface mounted CFRP laminates. In: Proc. 7th International Symposium on Fiber-Reinforced Polymer Reinforcement for Concrete Structures (SP:230-45), American Concrete Institute. 2005;779-794.
8. Rahimi H, Hutchinson A. Concrete beams strengthened with externally bonded FRP plates. Journal of Composites for Construction. 2001;5:44-56.
9. Ross CA, Jerome DM, Tedesco JW, Hughes ML. Strengthening of reinforced concrete beams with externally bonded composites laminates. ACI Structural Journal. 1999;96:212-220.
10. Ramana VPV, Kant T, Morton SE, Dutta PK, Mukherjee A, Desai YM. Behavior of CFRPC strengthened reinforced concrete beams with varying degrees of strengthening. Composites Part B: Engineering. 2000;31:461-470.
11. Katsumata H, Kobatake Y, Takeda T. A study with carbon fiber for earthquake-resistant capacity of existing reinforced concrete columns. In: Proc. Proceedings of the Ninth World Conference on Earthquake Engineering, Tokyo - Kyoto, Japan. 1988;517-522.
12. Triantafillou TC. Strengthening of structures with advanced FRPs. Progress in Structural Engineering and Materials. 1998;1:126-134.
13. David E, Djelal C, Buyle-Bodin F. Repair and strengthening of reinforced concrete beams using composite materials. In: Proc. 2nd Int PhD Symposium in Civil Engineering, Budapest; 1998.
14. Shahawy MA, Arockiasamy M, Beitelman T, Sowrirajan R. Reinforced concrete rectangular beams strengthened with CFRP laminates. Composites Part B: Engineering. 1996;27:225-233.
15. Khalifa A, Nanni A. Rehabilitation of rectangular simply supported RC beams with shear deficiencies using CFRP composites. Construction and Building Materials. 2002;16:135-146.
16. Shehata AEM, Cerqueira EC, Pinto CTM. Coppe, strengthening of RC beams in flexure and shear using CFRP laminate. In: C.J. Burgoyne (Ed.) FRPRCS-5: Fibre-reinforced Plastics for Reinforced Concrete Structures: Proceedings of the Fifth International Conference on Fibre-Reinforced Plastics for Reinforced Concrete Structures, Cambridge, UK, 16-18 July, Thomas Telford. 2001;97-106.
17. Khalifa A, Tumialan G, Nanni A, Belarbi A. Shear strengthening of continuous RC

beams using externally bonded CFRP sheets. In: Proc. Proceedings of the 4th International Symposium on FRP for Reinforcement of Concrete Structures (FRPRCS4), American Concrete Institute, Baltimore, MD. 1999;995-1008.
18. Saadatmanesh H, Ehsani MR. RC beams strengthened with GFRP plates. I: Experimental Study Journal of Structural Engineering. 1991;117:3434-3455.
19. Meier U, Kaiser H. Strengthening of structures with CFRP laminates. In: Proc. Advanced Composites Materials in Civil Engineering Structures, Flamingo Hilton, Las Vegas, Nevada, United States. 1991;224-232.
20. Jumaat MZ, Alam MA. Optimization of intermediate anchors to eliminate premature shear failure of CFRP laminate flexurally strengthened R.C beams. International Journal of Physical Science. 2011;6:182-192.
21. Jumaat MZ, Rahman MA, Alam MA, Rahman MM. Premature failures in plate bonded strengthened RC beams with an emphasis on premature shear: A review. International Journal of Physical Science. 2011;6:156-168.
22. Alam MA, Jumaat MZ. Eliminating premature end peeling of flexurally strengthened reinforced concrete beams. Journal of Applied Sciences. 2009;9:1106-1113.
23. Aram MR, Czaderski C, Motavalli M. Debonding failure modes of flexural FRP-strengthened RC beams. Composites Part B: Engineering. 2008;39:826-841.
24. Yao J, Teng JG. Plate end debonding in FRP-plated RC beams—I: Experiments. Engineering Structures. 2007;29:2457-2471.
25. Karunasena W, Hardeo P, Bosnich G. Rehabilitation of concrete beams by externally bonding fibre composite reinforcement. In: Proc. Proceeding of the 4th International Composites Conference (ACUN-4), Sydney, Australia. 2002;222-226.
26. Kachlakev D, McCurry DD. Behavior of full-scale reinforced concrete beams retrofitted for shear and flexural with FRP laminates. Composites Part B: Engineering. 2000;31:445-452.
27. Toutanji H, Zhao L, Zhang Y. Flexural behavior of reinforced concrete beams externally strengthened with CFRP sheets bonded with an inorganic matrix. Engineering Structures. 2006;28:557-566.
28. Ferreira AJM. On the shear-deformation theories for the analysis of concrete shells reinforced with external composite laminates. Strength of Materials. 2003;35: 128-135.
29. Zhang AH, Jin WI, Li GB. Behavior of preloaded RC beams strengthened with CFRP laminates. J. Zhejiang Univ. - Sci. A. 2006;7:436-444.
30. Wenwei W, Guo L. Experimental study of RC beams strengthened with CFRP sheets under sustaining loads. J. Wuhan Univ. Technol.-Mat. Sci. Edit. 2006;21:82-85.
31. Ashour AF, El-Refaie SA, Garrity SW. Flexural strengthening of RC continuous beams using CFRP laminates. Cement and Concrete Composites. 2004;26:765-775.
32. Wang J, Zhang C. Nonlinear fracture mechanics of flexural–shear crack induced debonding of FRP strengthened concrete beams. International Journal of Solids and Structures. 2008;45:2916-2936.
33. Wenwei W, Guo L. Experimental study and analysis of RC beams strengthened with CFRP laminates under sustaining load. International Journal of Solids and Structures. 2006;43:1372-1387.
34. Obaidat YT. Retrofitting of reinforced concrete beams using composite laminate. Master Thesis, Jordan University of Science and Technology; 2007.
35. Ahmed E, Sobuz HR, Sutan NM. Flexural performance of CFRP strengthened RC beams with different degrees of strengthening schemes. International Journal of the Physical Sciences. 2011;6: 2229-2238.
36. Sobuz HR, Ahmed E. Flexural performance of RC beams strengthened with different reinforcement ratios of CFRP laminates. Key Engineering Materials. 2011;471-472:79-84.
37. Jumaat MZ, Alam MA. Experimental and numerical analysis of end anchored steel plate and CFRP laminate flexurally strengthened RC beams. International Journal of Physical Science. 2010;5:132-144.
38. Jumaat MZ, Rahman MM, Alam MA. Flexural strengthening of RC continuous T beam using CFRP laminate: A review. International Journal of Physical Science. 2010;5:619-625.

39. Barris C, Torres L, Turon A, Baena M, Catalan A. An experimental study of the flexural behaviour of GFRP RC beams and comparison with prediction models. Composite Structures. 2009;91:286-295.
40. Dash N. Strengthening of reinforced concrete beams using glass fiber reinforced polymer composites. (MTech) National Institute of Technology, Rourkela, India; 2009.
41. Esfahani MR, Kianoush MR, Tajari AR. Flexural behaviour of reinforced concrete beams strengthened by CFRP sheets. Engineering Structures. 2007;29:2428-2444.
42. Teng JG, Smith ST, Yao J, Chen JF. Intermediate crack-induced debonding in RC beams and slabs. Construction and Building Materials. 2003;17:447-462.
43. Naji HF, Abdulrahman SK, Abass HE. Shear behavior of RC beams strengthened with varying types of FRP materials using finite element analysis. Journal of Engineering and Development. 2011;15: 183-204.
44. Abbas JL, Abd SM. Shear capacity and deflection response of RC beams strengthened in shear with U-shaped CFRP wraps. European Journal of Scientific Research. 2012;82:265-282.
45. Guo Z, Cao S, Sun W, Lin X. Experimental study on bond stress-slip behaviour between FRP sheets and concrete. In: Proc. Proceedings of the International Symposium on Bond Behaviour of FRP in Structures, International Institute for FRP in Construction. 2005;77-84.
46. Ebead UA, Marzouk H. Tension-stiffening model for FRP-strenghened RC concrete two-way slabs. Materials and Structures. 2005;38:193-200.
47. Comité Euro-International du Béton, CEB-FIP Model Code 1990 Thomas Telford services Ltd., London; 1993.
48. Piggott M. Load bearing fibre composites, 2nd ed. Kluwer Academic Publishers, New York/Boston/Dordrecht/London/Moscow; 2002.
49. Simulia DS. ABAQUS 6.11 Documentation, DS SIMULIA Corp, Providence, RI, USA; 2011.
50. Benzeggagh ML, Kenane M. Measurement of mixed-mode delamination fracture toughness of unidirectional glass/epoxy composites with mixed-mode bending apparatus. Composites Science and Technology. 1996;56:439-449.
51. Lubliner J, Oliver J, Oller S, Oñate E. A plastic-damage model for concrete. International Journal of Solids and Structures. 1989;25:299-326.
52. Coronado CA, Lopez MM. Sensitivity analysis of reinforced concrete beams strengthened with FRP laminates. Cement and Concrete Composites. 2006;28:102-114.
53. Qiao P, Chen Y. Cohesive fracture simulation and failure modes of FRP–concrete bonded interfaces. Theoretical and Applied Fracture Mechanics. 2008;49: 213-225.
54. Lundqvist J, Nordin H, Täljsten B, Olofsson T. Numerical analysis of concrete beams strengthened with CFRP: A study of anchorage lengths. In: Proc. Proceedings of BBFS: International Symposium on Bond Behaviour of FRP in Structures (BBFS 2005), International Institute for FRP in Construction, Hong Kong, China. 2005;247-254.
55. Hashemi SH, Maghsoudi AA, Rahgozar R. Bending response of HSRC beams strengthened with FRP sheets. SCIENTIA IRANICA. 2009;16:138-146.
56. Emadi J, Hashemi SH. Flexural study of high strength RC beams strengthened with CFRP plates. World Academy of Science, Engineering and Technology, International Science Index. 2011;54(5):327-331.

Peer-review history:
The peer review history for this paper can be accessed here:
http://www.sdiarticle3.com/review-history/19609